1.82-μm distributed feedback lasers with InGaAs/InGaAsP multiple-quantum wells for a H_2O sensing system

Hongyan Yu (于红艳), Jiaoqing Pan (潘教青)*, Yongbo Shao (邵永波), Baojun Wang (王宝军), Daibing Zhou (周代兵), and Wei Wang (王 圩)

Key Laboratory of Semiconductor Materials Science, Institute of Semiconductors, Chinese Academy of Sciences, Beijing 100083, China

**Corresponding author: jqpan@semi.ac.cn*

Received September 22, 2012; accepted October 10, 2012; posted online February 6, 2013

High-strained InGaAs/InGaAsP multiple quantum wells (MQWs) distributed feedback (DFB) lasers, fabricated using metal organic chemical vapor deposition, are presented at 1.82 μm with a high side-mode-suppression ratio of 49.53 dB. The current- and temperature-tuning rates of the DFB mode wavelength are 0.01 nm/mA and 0.13 nm/°C, respectively. A characteristic temperature of 51 K is also confirmed. The DFB laser demonstrates good performance and can be applied to H_2O concentration sensing.

OCIS codes: 140.0140, 140.5960, 140.3070, 140.3490.
doi: 10.3788/COL201311.031404.

Recently, near infrared lasers with an emission wavelength range of 1.6–2.1 μm have gained interest due to their applications in light sources of gas sensing. Such interest is due to the strong absorption lines of various gases, such as CH_4 (1.665 μm), HCl (1.743 μm), and NO (1.795 μm), in this wavelength range. Specifically, H_2O has absorption lines at wavelengths around 1.82 μm (Fig. 1). Therefore, the distributed feedback (DFB) lasers with a strained multiple quantum wells (MQWs) structure, which can operate in the 1.6−2.1-μm wavelength range, has recently attracted much interest[1−4]. High-strained InGaAs/InGaAsP MQW DFB laser, with the grating fabricated in the active region, can produce a stable single-mode operation with the linewidth of several megahertzs that is narrower than the absorption linewidth of gas molecules (hundred megahertzs). The temperature and drive current are employed to tune the lasing mode to the precise absorption lines of the target gases. The InGaAs/InGaAsP MQW DFB laser is a suitable light source of tunable diode laser absorption spectroscopy (TDLAS) for gas sensor systems.

The emission wavelength of compressively strained InGaAs quantum well material can be extended to nearly 2 μm by increasing the strain and the well thickness. However, the large strain in the MQW structure generates unwanted crystalline defects owing to the three-dimensional (3D) growth of the well. In addition, the interband absorption and Auger recombination[5] increase distinctly with the extension of the emission wavelength. Although researchers have spent much effort studying unconventional wavelengths, satisfactory performance is seldom achieved. In this letter, we employ 10-s growth interruption in the InP buffer layer to improve the quality of large strained MQW structure. At present, single-mode DFB GaInSb lasers emitting at 1.877 μm and often used for sensitive detection of H_2O concentrations, have been fabricated by Nanoplus GmbH[6]. Nevertheless, there are hardly any reports of a DFB InGaAs laser emitting at the wavelength from 1.8 to 1.9 μm for H_2O sensing. Compared with the dew-point hygrometer with sensitivity of parts per million (ppm) levels, the H_2O sensing system based on DFB laser sources can enhance the detection sensitivity to parts per billion (ppb) levels using TDLAS techniques. Thus, we fabricated 1.82-μm DFB InGaAs lasers corresponding to the absorption lines of water vapor for sensitive detection of H_2O concentrations.

In this letter, the epitaxial layers were grown on an n-InP substrate by low pressure metal organic chemical vapor deposition (MOCVD) with a horizontal reaction chamber. The growth pressure and temperature were 22 mbar and 655 °C, respectively, throughout the entire growth processes. The reactants used were Trimethyl-indium (TMIn) and Trimethyl-gallium (TMGa) as the group-III sources, arsine (AsH_3) and phosphine (PH_3) as the group-V sources, and purified H_2 as the carrier gas for the TMIn and TMGa. SiH_4 and DEZn were employed as n-type and p-type dopants, respectively.

The 10-s growth interruption in the InP buffer layers was employed to improve the quality of epitaxial layers[7]. The active region consisted of four 1.2% compressively strained 8.4-nm $In_{0.71}Ga_{0.29}As$ quantum wells and five –0.25% tensilely strained 13.8-nm InGaAsP barriers exhibiting room temperature (RT) photoluminescence (PL) peak at 1.825 μm. The MQWs adopted strain-compensated structure, and the barriers also acted as

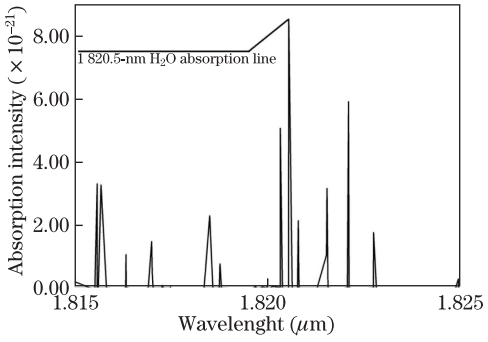

Fig. 1. Absorption spectra of H_2O extracted from the HITRAN database.

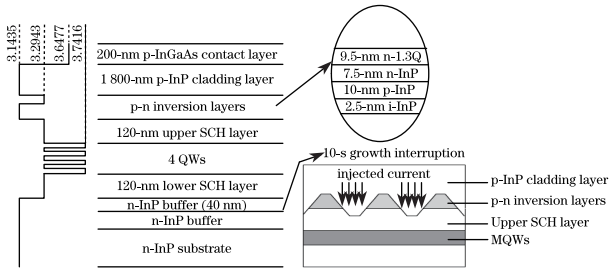

Fig. 2. Epitaxial layer with corresponding refractive index and grating structure.

carrier-blocking layers, which prevented carrier leakage from the quantum well and enhanced the temperature stability. The wells and barriers were embedded in two 120-nm-thick, 1.3 Q lattice-matched InGaAsP waveguide layers (band-gap wavelength: 1.3 μm) to form a separate-confinement heterostructure (SCH) MQW structure. P-n inversion layers that induced complex coupling gain into the DFB structure were grown on the upper SCH layer in order to improve the single mode property. First-order grating corrugations were etched into the p-n inversion layers and into the top of SCH layer by conventional holographic exposure and usual photolithography. Afterwards, the subsequent regrowth, consisting of a p-InP cladding layer and a p-InGaAs contact layer, was implemented. The epitaxial layer with corresponding refractive index and grating structure are shown in Fig. 2. After regrowth, a ridge waveguide with a width of 3 μm was fabricated by removing the p-cladding and p^+-contact layers using conventional photolithography and wet chemical etching. Ti-Pt-Au was used for P-contact metallization. N-metallization (AuGeNi/Au) was deposited onto the bottom side of the wafer after substrate thinning and polishing. Lasers with a length of 300 μm were cleaved and separated into individual chips. The laser chips were mounted P-side up on Cu heatsinks for continuous-wave (CW) operation.

The Fabry-Perot (FP) lasers were fabricated by the same processes, but without grating in order to facilitate wafer quality evaluation and the optimization of growth conditions. The peak wavelength was set at 1.82 μm at the injection current of 60 mA. Next, the DFB laser with grating period Λ of 281.23 nm, duty cycle of 50%, and a depth of 70 nm was fabricated. The inset (a) of Fig. 3 demonstrates the spectrum with an emission wavelength of 1.795 μm under a CW operation current of 70 mA at RT. The wavelength of the DFB mode is shorter than the FP mode due to fact that the grating period fabricated is less than that of our design. The device maintains single-mode operation at a large current range. The CW light-current ($L-I$) characteristics of uncoated device at different temperatures (from −20 to 50 °C are shown in Fig. 3). At 20 °C the threshold current is 19.7 mA, and the 9.9-mW output power per facet is achieved without saturation. As the temperature increases, the $I_{\rm th}$ and $P_{\rm out}$ degenerate owing to the temperature-dependent nonradiative recombination. The inset (b) of Fig. 3 shows the threshold current dependence on the operation temperature. By analyzing the data with the empirical relation, $I_{\rm th} = I_0 \exp(T/T_0)$, the characteristic temperature T_0 is estimated to be 58 K, which is comparable to that of a conventional 1.55-μm DFB laser. We know that Auger recombination is very important in the decreasing band gap, because it can lead to a deterioration of the temperature stability of long wavelength lasers[8]. In this letter, the relatively high barrier height prevents carrier overflow from the quantum well. Thus, the device shows good temperature stability.

The first-order Bragg grating period was increased to 285.51 nm to yield an output wavelength λ_0 of 1.82 μm ($\lambda_0 = 2n_{\rm eff}\Lambda$). The emission spectrum of the device taken at 25 °C under a CW operation current of 90 mA is shown in Fig. 4. The DFB mode has a wavelength of 1 819 nm with a side-mode-suppression ratio (SMSR) of 49.53 dB. This value is considered the highest when compared with the long-wavelength lasers reported in earlier works. The coupling coefficient is estimated to be 92 $\rm cm^{-1}$ from the measured stop-band width of 4.37 nm for the DFB laser with a length of 300 μm. The complex coupled grating was formed sinusoidally in favor of regrowth (Fig. 4, inset). The current- and temperature-tuning rates of the DFB mode wavelength are 0.01 nm/mA and 0.13 nm/°C respectively (Fig. 5). Meanwhile, Fig. 6 shows the $L-I$ characteristic of 2 uncoated DFB laser chips (i.e., A1 and A2) with a length of 300 μm. The $L-I$ lines actually contain some dips with different amplitudes, which can be attributed to the absorption of light by water vapor in the air. The laser is tuned across several absorption peaks of water vapor when adjusting the drive current, because there are dense H_2O absorption lines in a small range of wavelength. Consequently, the absorption dips are observed in the $L-I$ curves as the output light of the laser passes through the air. The

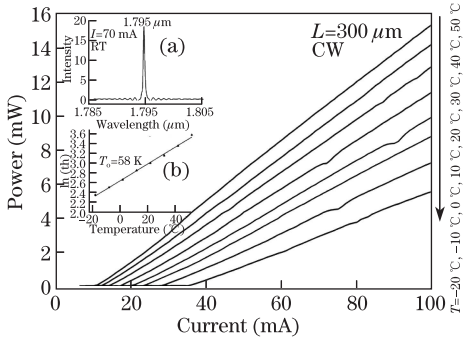

Fig. 3. CW $L-I$ characteristics of 1.795-μm DFB laser taken for heat sink temperatures between –20 to 50 °C. Insets show (a) the emission spectrum and (b) the threshold current dependence on mount temperature.

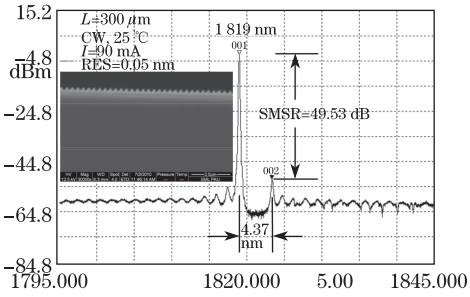

Fig. 4. Emission spectrum of 1.82-μm DFB laser with a CW operation current of 90 mA at 25 °C. Inset shows SEM image of the cross section of the grating.

individual peaks of the H_2O absorption spectra have different absorption intensities, that is, the amount of power absorbed varies accordingly if the wavelength of the light is changed. As such, the amplitudes of the dips are different, and the centers of the dips represent the wavelength of interest. Depending on the Lambert-Beer law, we can measure the water vapor concentration using absorption spectroscopy technique with a DFB laser as light source. The details of the H_2O sensor system will be studied and reported in the future. The threshold current and output power at 100 mA of the DFB laser chip A1 are 18.9 mA and 9.54 mW, respectively. In order to investigate long-term reliability, we performed aging test on the chips under a constant driving current of 150 mA at 100 °C for 24 h. Given that degradation is not observed, the proposed DFB laser is a practical light source for H_2O sensor applications. Finally, the DFB chip was presented in an industry standard hermetically sealed 14-pin butterfly integrated with optical isolator, thermo-electric cooler (TEC), thermistor, and power monitor photodiode. Before being sealed, the rear facet of the laser received a high reflection ($Rr = 85\%$) coating, and the front facet of the laser was anti-reflection ($Rf = 1\%$) coated. Figure 7 shows images of the laser and CW fiber output power versus current characteristics at different temperatures. A threshold current of 25.5 mA and a fiber output power of 4.3 mW at module temperature of 25 °C are achieved. The operating temperature that is dependent on threshold current is plotted in the inset of Fig. 7. The value of T_0 is estimated to be 51 K at RT, which is worse than the value of 1.795 μm generated by the DFB laser. The observed stronger temperature dependence of the threshold current on longer wavelength semiconductor lasers has focused attention on the Auger effect[9−11]. Overall, the 1.82-μm DFB laser exhibits good performance and has promising practical applications.

In conclusion, we fabricate and test high-strained InGaAs/InGaAsP MQW DFB lasers with a compressive strain of 1.2%. The lasing wavelength is 1.82 μm with a high SMSR of 49.53 dB. The lasers can be well controlled by the temperature at the rate of 0.13 nm/°C and by the injection current at the rate of 0.01 nm/mA. Furthermore, a threshold current of 18.9 mA and a CW output power of 9.54 mW under an operation current of 100 mA are achieved at RT for the uncoated device with a length of 300 μm. The $L - I$ curve contains some dips

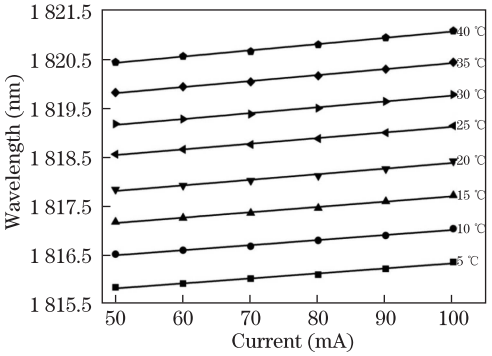

Fig. 5. Dependence of 1.82-μm DFB mode wavelength on injection current at temperatures of 5–40 °C.

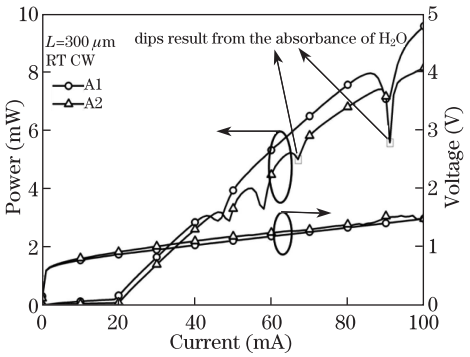

Fig. 6. CW $L - I$ characteristics of 1.82-μm DFB chips at RT.

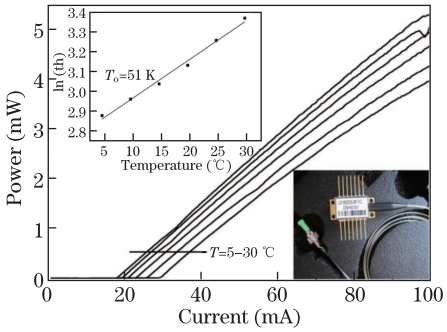

Fig. 7. CW $L - I$ characteristics of 1.82-μm DFB laser after butterfly packaging taken from 5 to 30 °C in a 5 °C step. Insets show the threshold current plotted as a function of operating temperature as well as a photograph of a 14-pin butterfly housing with FC/APC fiber.

where the water vapor in the air absorbed at the wavelength corresponding to the laser current. We also perform aging tests on the DFB lasers under a constant drive current of 150 mA at 100 °C for 24 h and observe no degradation. The CW fiber output power of the butterfly housing laser can achieve 4.3 mW under 100-mA operation current at a temperature of 25 °C a characteristic temperature of 51 K is also confirmed. Finally, we demonstrate that the DFB laser is a practical light source for H_2O sensor applications.

This work was supported by the National "863" Project of China (No. 2012AA012203) and the National "973" Program of China (No. 2011CB301702).

References

1. T. Sato, M. Mitsuhara, T. Watanabe, K. Kasaya, T. Takeshita, and Y. Kondo, IEEE J. Sel. Topics Quantum Electron. **13,** 1079 (2007).
2. R. Phelan, J. O'Carroll, D. Byrne, C. Herbert, J. Somers, and B. Kelly, IEEE Photon. Technol. Lett. **24,** 652 (2012).
3. A. V. Lyutetskii, N. A. Pikhtin, S. O. Slipchenko, Z. N. Sokolova, N. V. Fetisova, A. Yu. Leshko, V. V. Shamakhov, A. Yu. Andreev, E. G. Golikova, Yu. A. Ryaboshtan, and I. S. Tarasov, Semiconductors **37,** 1356 (2003).
4. Y. Zhang, Y. Zheng , C. Lin, A. Li, and S. Liu, Chin. Phys. Lett. **23,** 2262 (2006).
5. B. L. GelMont, Z. N. Sokolova, and I. N. Yassievich, Sov. Phys. Semicond. **16,** 382 (1982).

6. T. Le Barbu, B. Parvitte, V. Zeninari, I. Vinogradov, O. Korablev, and G. Durryet, Appl. Phys. B **82,** 133 (2006).
7. F. Bugge, G. Beister, G. Erbert, S. Gramlich, I. Rechenberg, H. Treptow, and M. Weyers, J. Cryst. Growth. **145,** 907 (1994).
8. N. F. Masse, A. R. Adams, and S. J. Sweeney, Appl. Phys. Lett. **90,** 161113 (2007).
9. N. K. Dutta and R. J. Nelson, Appl. Phys. Lett. **38,** 407 (1981).
10. A. Sugimura, IEEE J. Quantum Electron. **17,** 627 (1981).
11. G. Fuchs, C. Schiedel, A. Hangleiter, V. Harle, and F. Scholz, Appl. Phys. Lett. **62,** 396 (1993).